

Cluster Analysis–Based Physiological Classification and Morphological Properties of Inhibitory Neurons in Layers 2–3 of Monkey Dorsolateral Prefrontal Cortex

Leonid S. Krimer, Aleksey V. Zaitsev, Gabriela Czanner, Sven Kröner, Guillermo González-Burgos, Nadezhda V. Povysheva, Satish Iyengar, German Barrionuevo and David A. Lewis

J Neurophysiol 94:3009-3022, 2005. First published Jun 29, 2005; doi:10.1152/jn.00156.2005

You might find this additional information useful...

This article cites 62 articles, 33 of which you can access free at:

<http://jn.physiology.org/cgi/content/full/94/5/3009#BIBL>

This article has been cited by 2 other HighWire hosted articles:

Correlation Between Axonal Morphologies and Synaptic Input Kinetics of Interneurons from Mouse Visual Cortex

D. Dumitriu, R. Cossart, J. Huang and R. Yuste
Cereb Cortex, January 1, 2007; 17 (1): 81-91.

[\[Abstract\]](#) [\[Full Text\]](#) [\[PDF\]](#)

Electrophysiological Classification of Somatostatin-Positive Interneurons in Mouse Sensorimotor Cortex

B. Halabisky, F. Shen, J. R. Huguenard and D. A. Prince
J Neurophysiol, August 1, 2006; 96 (2): 834-845.

[\[Abstract\]](#) [\[Full Text\]](#) [\[PDF\]](#)

Updated information and services including high-resolution figures, can be found at:

<http://jn.physiology.org/cgi/content/full/94/5/3009>

Additional material and information about *Journal of Neurophysiology* can be found at:

<http://www.the-aps.org/publications/jn>

This information is current as of December 15, 2006 .

Cluster Analysis–Based Physiological Classification and Morphological Properties of Inhibitory Neurons in Layers 2–3 of Monkey Dorsolateral Prefrontal Cortex

Leonid S. Krimer,¹ Aleksey V. Zaitsev,¹ Gabriela Czanner,² Sven Kröner,³ Guillermo González-Burgos,¹ Nadezhda V. Povysheva,¹ Satish Iyengar,² German Barrionuevo,³ and David A. Lewis^{1,3}

¹Departments of Psychiatry, ²Statistics, and ³Neuroscience, University of Pittsburgh, Pittsburgh, Pennsylvania

Submitted 14 February 2005; accepted in final form 27 June 2005

Krimer, Leonid S., Aleksey V. Zaitsev, Gabriela Czanner, Sven Kröner, Guillermo González-Burgos, Nadezhda V. Povysheva, Satish Iyengar, German Barrionuevo, and David A. Lewis. Cluster analysis–based physiological classification and morphological properties of inhibitory neurons in layers 2–3 of monkey dorsolateral prefrontal cortex. *J Neurophysiol* 94: 3009–3022, 2005. First published June 29, 2005; doi:10.1152/jn.00156.2005. In primates, little is known about intrinsic electrophysiological properties of neocortical neurons and their morphological correlates. To classify inhibitory cells (interneurons) in layers 2–3 of monkey dorsolateral prefrontal cortex we used whole cell voltage recordings and intracellular labeling in slice preparation with subsequent morphological reconstructions. Regular spiking pyramidal cells have been also included in the sample. Neurons were successfully segregated into three physiological clusters: regular-, intermediate-, and fast-spiking cells using cluster analysis as a multivariate exploratory technique. When morphological types of neurons were mapped on the physiological clusters, the cluster of regular spiking cells contained all pyramidal cells, whereas the intermediate- and fast-spiking clusters consisted exclusively of interneurons. The cluster of fast-spiking cells contained all of the chandelier cells and the majority of local, medium, and wide arbor (basket) interneurons. The cluster of intermediate spiking cells predominantly consisted of cells with the morphology of neurogliaform or vertically oriented (double-bouquet) interneurons. Thus a quantitative approach enabled us to demonstrate that intrinsic electrophysiological properties of neurons in the monkey prefrontal cortex define distinct cell types, which also display distinct morphologies.

INTRODUCTION

The intrinsic electrophysiological properties of individual cortical neurons strongly influence their input–output relationships (Nowak et al. 2003) and play an important role in information processing in cortical circuits (Magee 2003). Studies of these properties can be traced to the original *in vivo* extracellular recordings, which suggested that cortical neurons could be segregated into regular-spiking (RS) and fast-spiking (FS) populations based on the width of their action potentials (Mountcastle et al. 1969; Simons 1978). More detailed studies of membrane properties in these cells have been conducted using intracellular recordings from a rodent cortical slice preparation (Connors and Gutnick 1990; McCormick et al. 1985), and such experiments demonstrated that RS and FS neurons correspond to pyramidal and nonpyramidal morphological types, respectively.

Subsequent studies of intrinsic electrophysiological properties further subdivided cortical interneurons as low threshold spiking (LTS), late spiking (LS), regular spiking nonpyramidal (RSNP), and irregular spiking (Cauli et al. 1997, 2000; Kawaguchi 1993, 1995; Kawaguchi and Kubota 1997). More recently, a classification scheme was developed based on the response to both the onset and steady-state step-current injections (Gupta et al. 2000; Markram et al. 2004).

Although some studies of interneurons have been able to correlate electrophysiological properties with specific morphological subtypes and/or the presence of specific calcium-binding proteins (Bacci et al. 2003; Blatow et al. 2003; Cauli et al. 1997; Chu et al. 2003; Gao et al. 2003; Gibson et al. 1999; Kawaguchi 1995; Rozov et al. 2001), others have not (Chitwood and Jaffe 1998; Parra et al. 1998; Porter et al. 2001).

The classification schemes adopted in most of the previous studies of neocortical neurons used somewhat arbitrary criteria to define boundaries between electrophysiological groups of neurons. Only few studies have used a quantitative multivariate classification approach based on cluster analysis. For example, one study successfully segregated RS and FS neurons (Nowak et al. 2003) in cat visual cortex. Another study classified fusiform interneurons in rat neocortex using a combination of electrophysiological and molecular parameters (Cauli et al. 2000).

Despite a substantial record of *in vivo* electrophysiological studies investigating the neural correlates of cognition and working memory in monkey (Constantinidis et al. 2002; Funahashi et al. 1989; Fuster 2001; Goldman-Rakic 1995; Miller 2000; Rao et al. 1999), the intrinsic membrane properties of these neurons and their relationships with morphology still remain largely unknown. In addition, direct extrapolation of the studies in rodents to primates is difficult considering substantial differences in the prefrontal cortex between these species [i.e., the proportions of chemically defined classes of interneurons (Conde et al. 1994; Gabbott and Bacon 1996; Gabbott et al. 1997; Kawaguchi and Kubota 1997) and developmental origin of interneurons (Letinic et al. 2002; Xu et al. 2004)].

We have recently adopted cluster analysis to correlate physiological membrane properties with the content of calcium-binding proteins in interneurons from the monkey dorsolateral prefrontal cortex (DLPFC; Zaitsev et al. 2005). However, in

Address for reprint requests and other correspondence: L. S. Krimer, Western Psychiatric Institute and Clinic, Biomedical Science Tower, W1651, 3811 O'Hara Street, Pittsburgh, PA 15213 (E-mail: krimerls@upmc.edu).

The costs of publication of this article were defrayed in part by the payment of page charges. The article must therefore be hereby marked "advertisement" in accordance with 18 U.S.C. Section 1734 solely to indicate this fact.

this study the relationship between physiological and morphological properties of these interneurons could not be adequately addressed. To preserve calcium-binding proteins in the recorded cells, we used short recording times (5–7 min; Kawaguchi 1995), which in turn precluded reliable morphological recovery of many interneurons. Therefore in the present subsequent study, we used long recording times to explore the correlation of physiological and morphological properties in large numbers of DLPFC interneurons ($n = 171$ and 159 , respectively). Furthermore, we have included data from morphologically identified regular spiking pyramidal cells to compare them to the various classes of interneurons. Multivariate statistical analysis of the large neuronal data set generated three physiological clusters of neurons. Different morphological classes of neurons showed large or complete overlap with one of the three physiological clusters.

METHODS

Tissue acquisition

DLPFC slices ($n = 192$) were obtained from 12 young adult (3.5–6 kg; 4- to 5-yr-old) male long-tailed macaque monkeys (*Macaca fascicularis*) treated according to the guidelines outlined in the National Institutes of Health Guide for the Care and Use of Laboratory Animals, as approved by the University of Pittsburgh Institutional Animal Care and Use Committee. Brain slices from these animals also were used in other studies both published (González-Burgos et al. 2005; Povysheva et al. 2005; Zaitsev et al. 2005) and ongoing. Animals were treated with ketamine hydrochloride (25 mg/kg, intramuscular [im]), dexamethasone phosphate (0.5 mg/kg, im), and atropine sulfate (0.05 mg/kg, subcutaneous); an endotracheal tube was inserted and anesthesia was maintained with 1% halothane in a 28% O₂–air mixture. Monkeys were placed in a stereotaxic apparatus and a craniotomy was performed over the DLPFC in one hemisphere. The dura was removed in a location determined by stereotaxic coordinates and by the position of relevant sulcal landmarks, and a small block of tissue was excised containing both the medial and lateral banks of the principal sulcus (area 46) as well as a small adjacent portion of dorsal area 9. After the surgery, the animals were treated with an antibiotic (chloramphenicol, 15 mg/kg, im) and an analgesic (hydromorphone, 0.02 mg/kg, im) three times a day for 3 days. All animals recovered quickly with no impairments in eating or drinking and no overt behavioral deficits. In most cases, the animals underwent the same procedure 2–4 wk later to obtain tissue from the opposite hemisphere. During the second procedure, after the craniotomy, the animal was given an overdose of pentobarbital (30 mg/kg) and was perfused through the heart with ice-cold modified artificial cerebrospinal fluid. A tissue block containing portions of areas 46 and 9 from a nonhomotopic portion of the contralateral hemisphere was quickly excised. Subsequent treatment of the tissue was the same for both procedures. Previous studies have demonstrated that the initial biopsy did not affect the properties of neurons obtained in the contralateral hemisphere (González-Burgos et al. 2000, 2004; Henze et al. 2000).

Preparation of brain slices

Through all steps of the experiment, tissue was maintained in Ringer solution of the same content (in mM): NaCl 126, KCl 2.5, NaH₂PO₄ 1.25, CaCl₂ 2, MgSO₄ 1, NaHCO₃ 26 and dextrose 10, pH 7.4 perfused with 95% O₂–5% CO₂ gas mixture. Multiple (usually 16) slices of 350 μ m thickness were cut in the coronal plane using a vibratome (VT 1000S, Leica, Wetzlar, Germany) and after 1-h recovery at 36°C they were submerged in a chamber, mounted on a Zeiss Axioscop 2 FS microscope (Oberkochen, Germany), and perfused

with Ringer solution at 32°C. Each experiment lasted ≤ 24 h as dictated by the survival of the slices.

Electrophysiology

Neurons in layers 2–3 were identified visually using infrared illumination and video-enhanced differential interference contrast optics (Stuart et al. 1993). Interneurons were identified based on their usually smaller cell body and lack of an apical dendrite. Pyramidal cells with regular spiking properties were also included in the sample. Patch electrodes with electrical resistances of 7–12 M Ω were pulled from borosilicate capillary glass and filled with a solution containing (in mM): potassium gluconate 114, KCl 6, ATP-Mg 4, GTP 0.3, Hepes 10, and pH 7.25 adjusted with KOH. Biocytin (0.5%; Molecular Probes, Eugene, OR) was added to the solution for subsequent morphological identification of the neurons. Whole cell voltage recordings were performed after reaching high resistance seal (≥ 5 G Ω). Access resistance was monitored and typically was 12–30 M Ω . Capacitance was compensated on-line. Voltages were amplified using Intracellular Electrometers IE-210 (Warner Instrument, Hamden, CT), operating in bridge-balance mode, and filtered on-line at 5 kHz. Data were acquired to a PC at sampling rates of 20 kHz by a Power 1401 interface using Signal 2 software (CED, Cambridge, UK). Intrinsic membrane properties were determined from the voltage responses elicited by injection of a series of hyper- and depolarizing current steps of 500-ms duration in 10- or 20-pA increments at 0.2 Hz with two repeats of each current step.

Physiological analysis

Input resistance was measured from the slope of a linear regression fit to the linear portion of the current–voltage relation near the end of the 500-ms step. Membrane time constant was determined by fitting a single exponential to the voltage response to hyperpolarizing current steps of -10 pA. Properties of single action potentials and spike trains were analyzed off-line using a Signal 2 script (CED). Properties of single action potentials were measured on the first spike evoked by the minimum current that reached the action potential threshold. Action potential threshold was determined as previously described (Henze et al. 2000), action potential amplitude was measured from the threshold to the peak, and action potential duration was measured at its half-amplitude. Amplitude of the fast component of the afterhyperpolarization (AHP_f) was measured from the action potential threshold to the hyperpolarization peak or, if present, to the onset of the slow component of the afterhyperpolarization (AHP_s). If an afterdepolarization (ADP) was present, its amplitude was determined as a distance between the peak of AHP_f to the peak of ADP. Amplitude of AHP_s was measured from the peak of ADP to the peak of AHP_s. If ADP was absent, amplitude of AHP_s was measured from the end of AHP_f. The latter was determined as the crossing point of two monoexponential curves fitted to AHP_f and AHP_s, respectively. The adaptation ratio of the first to last interspike interval was used to quantify a degree of spike adaptation within a sweep (Porter et al. 2001). For this measure we chose a sweep that was evoked by a depolarizing current step of 60 pA above the threshold for the first spike for each cell. Changes in the adaptation ratio across the 10- to 120-pA suprathreshold current range were also calculated using linear regression analysis (slope of adaptation ratio).

Statistical analysis

We used cluster analysis (Hand 1981; Johnson and Wichern 1998) on the following variables to divide the neurons into groups: input resistance; membrane time constant; action potential amplitude and duration; amplitudes of AHP_f, AHP_s, and ADP; and adaptation ratio and slope of adaptation ratio. Resting membrane potential and action potential threshold were not included because in our previous studies

they did not differ between the groups of interneurons (Gonzalez-Burgos et al. 2004; Zaitsev et al. 2005). Similarly, previous studies did not report differences in these measurements between pyramidal cells and subtypes of interneurons (Cauli et al. 1997; Krimer and Goldman-Rakic 2001; Porter et al. 2001). Mean values of resting membrane potential and action potential threshold are listed for each of the physiological clusters (Table 2), as well as for morphologically identified interneurons (Table 3). To create clusters, Ward's hierarchical clustering algorithm with Euclidean distance was used. The result of the clustering was plotted as a hierarchical tree or dendrogram. The vertical axis denotes the linkage (between-cluster) distance. Statistical significance of between-group differences/similarities was evaluated using ANOVA and Fisher's post hoc test for least-significant difference in multiple comparisons. Statistical analyses were performed using Statistica 6.1 software (StatSoft, Tulsa, OK). Unless stated otherwise, all data are reported as means and SDs.

Histological processing and neuronal reconstructions

After recordings, slices were fixed in cold 4% paraformaldehyde for 72 h, transferred into an antifreeze solution (one-to-one mixture of glycerol and ethylene glycol in 0.1 M phosphate buffer), and stored at -80°C . Slices were then cut into $5 \times 60\text{-}\mu\text{m}$ sections on a vibratome, reacted with 1% H_2O_2 , and placed in blocking serum with 0.5% Triton X-100 for 2 h at room temperature. Biocytin-labeled neurons were incubated with ABC-peroxidase and developed using the Ni-enhanced DAB chromogen. Interneurons were reconstructed using the NeuroLucida tracing system (MicroBrightField, Williston, VT) on an Axioplan 2 Zeiss microscope equipped with DIC, a $100 \times 1.4\text{NA}$ planapochromatic lens and additional Optovar magnification of $1.6 \times$ (final optical magnification of $1,600\times$; screen magnification of $7,200\times$). Characteristic features of the axonal arbor were used to identify the morphological types of reconstructed interneurons as previously described (Lund and Lewis 1993). The horizontal extent of axons was measured as the averaged distance between the three most distal axonal endings on each side from the soma of individual interneurons.

RESULTS

Qualitative description of electrophysiological membrane properties of neurons

A total of 219 cells were analyzed. Only two measures (i.e., resting membrane potential and action potential threshold) showed small coefficients of variance (CV) (8.6 and 13.4%, respectively), and normal distributions ($P = 0.27$ and 0.12 , respectively, Shapiro-Wilk W test). Each of the other membrane properties (see METHODS) had a larger CV and did not show a normal distribution ($P < 0.05$, Shapiro-Wilk W test). For example, spike amplitude and spike duration had CV values of 27 and 40%, respectively. The distribution histograms of these two measures suggested the presence of several subgroups of neurons (Fig. 1, A and B), although the absence of clear points of rarity in the distributions made it difficult to classify neurons based on a single physiological measure.

Consequently, we sought to determine whether particular combinations of membrane properties might distinguish neuronal populations, as has been suggested in studies of rodents (Kawaguchi 1995; McCormick et al. 1985). Therefore we calculated correlation coefficients to test whether any of the measures were correlated. A weak-to-moderate correlation was found between many variables (Table 1). The strongest correlations involved action potential duration, spike amplitude,

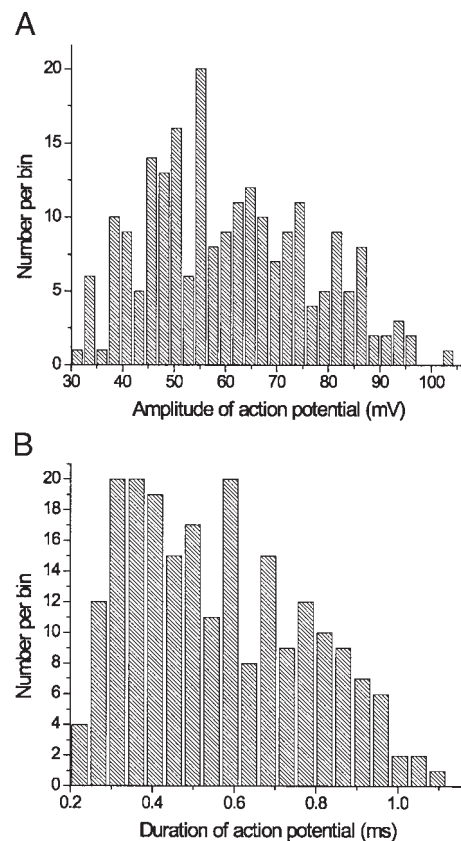


FIG. 1. Distribution histograms for the amplitude (A) and duration (B) of action potentials recorded in dorsolateral prefrontal cortex (DLPFC) cortical neurons. Both histograms suggest the presence of several subgroups of neurons, although the boundaries between the subgroups are obscured because of a considerable overlap of values in the potential subgroups of neurons.

amplitudes of AHPf and ADP, and adaptation ratio. Combinations of these measures were especially helpful in qualitatively distinguishing the RS and FS physiological groups of neurons in monkey DLPFC. Typical RS cells displayed a low input resistance and a long membrane time constant (Fig. 2, A and D), and generated action potentials with large amplitude and duration (Fig. 3D). Spike AHP of these cells had the shallowest fast component and was separated from the prominent slow component by marked ADP (Fig. 3A). These cells required strong depolarizing current to reach spike threshold (Figs. 2A and 4A). Once the threshold was reached, RS cells generated trains of spikes with low frequencies and prominent frequency adaptation (Fig. 4, A and D). The latter, almost invariably further increased with an increase in intensity of the stimulating current (Fig. 4D). Typically, FS neurons had input resistances that were slightly higher than those in RS cells, but the membrane time constant in FS cells was lower than that in the former (Fig. 2, C and D). Action potentials in FS neurons had small amplitudes and short durations (Fig. 3F). The AHP in FS cells had a prominent fast component and usually lacked the slow component or ADP (Fig. 3C). FS cells, compared with RS neurons, required fewer depolarizing current steps to reach spike threshold (Figs. 2C and 4C). Once threshold was reached, FS cells generated trains of spikes with high frequencies and small, if any, frequency adaptation. The latter usually was stable across the intensity range of the stimulating current (Fig. 4, C and F). Finally, we observed many neurons in which

TABLE 1. Significant correlations of the physiological parameters

No.	Variable	1	2	3	4	5	6	7	8	9	10
1	RMP, mV										
2	RI, mΩ	0.22									
3	TC, ms		0.32								
4	APT, mV	-0.17									
5	APA, mV			0.28							
6	APD, ms			0.43		0.37					
7	AHPAf, mV			-0.15	0.26	-0.26	-0.51				
8	AHPAs, mV			0.16		0.20		-0.40			
9	ADPA, mV		-0.27			0.47	0.15	-0.17			
10	AR					-0.23	-0.47	0.48		-0.22	
11	Slope × 10 ⁻³	0.20		-0.15		-0.17	-0.29	0.30	-0.34	-0.22	0.26
12	TTP, ms		-0.22	0.19	0.17				0.20		0.36

Statistical significance at $P < 0.05$. $n = 171$ neurons. RMP, resting membrane potential; RI, input resistance; TC, time constant (of membrane); APT, APA, and APD, threshold, amplitude, and duration of action potential; AHPAf and AHPAs, fast and slow components of afterhyperpolarization amplitude; ADPA, amplitude of afterdepolarization; AR and Slope, adaptation ratio and its change across the stimulating current range; TTP, time to first peak in a first suprathreshold sweep.

a combination of many physiological properties (such as time constant, spike duration, spike amplitude, and amplitude of AHPf) were intermediate between RS and FS cells (Figs. 2D and 3, B and E). This group of neurons seemed to correspond to the description of regular-spiking nonpyramidal cells in rat frontal cortex (Kawaguchi and Kubota 1997).

Physiological classification of the neurons using cluster analysis

To determine whether the electrophysiological properties of RS, FS, and neurons with the intermediate properties described above were part of a continuum from RS to FS, or could be segregated using a multivariate statistical approach, we used a cluster analysis for 171 of the 219 neurons. The remaining 48 neurons were excluded because of at least one missing value. We included physiological measures listed in the METHODS section. Because many variables were correlated with each other (Table 1), the cluster analysis on the original measures (standardized physiological measures) was compared with the cluster solution on the principal components (uncorrelated linear combinations of the correlated physiological measures). Both procedures yielded similar results; therefore the cluster solution for the original measures is reported here. The dendrogram obtained through Ward's hierarchical clustering algorithm revealed several clusters (Fig. 5), demonstrating the

presence of distinct physiological groups of neurons. The three criteria, pseudo F, pseudo t_2 , and cubic clustering criterion, which were applied to explore the potential number of clusters, suggested three clusters. Nonhierarchical k-means method also supported the Ward's clustering solution (Hand 1981; Johnson and Wichern 1998). The mean values of the physiological measures in the clusters (Table 2) corresponded well to the RS, FS, and regular-spiking nonpyramidal cells described in the rodent neocortex (Kawaguchi and Kubota 1997; McCormick et al. 1985). The cluster that had many membrane properties intermediate between RS and FS cells was designated as intermediate-spiking cells (IS). However, we chose to avoid the term "regular-spiking nonpyramidal cells" because it requires prior knowledge of the nonpyramidal morphology of these neurons. To contrast it with the cluster of FS cells, the combination of RS and IS physiological properties was designated as a nonfast-spiking (NFS) cluster. To determine how the corresponding variables differed between the three clusters, ANOVA and Fisher LSD post hoc tests were applied. RS, IS, and FS clusters differed from each other in amplitude and duration of the action potential, amplitude of AHPf, adaptation ratio, and slope of the adaptation ratio. Action potential duration appeared to be the most discriminating parameter with an F-ratio almost three times larger than for any other measure. The remaining measures differed only between any of two, but not all three, of the clusters (Table 2).

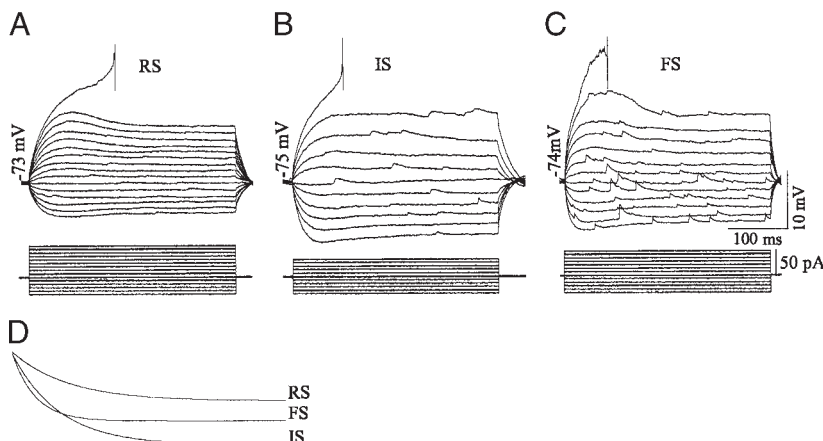


FIG. 2. Passive membrane properties of the typical regular-, intermediate-, and fast-spiking neurons (RS, IS, and FS, respectively) in monkey DLPFC. A: RS neuron displays low input resistance and requires the largest amplitude of depolarization current to reach action potential threshold. B: IS has the largest input resistance and requires the lowest amplitude of depolarization current to reach action potential threshold. C: FS displays the properties intermediate between the RS and IS. D: monoexponential curve fittings to the first hyperpolarizing sweeps demonstrates longest, intermediate, and shortest time constant in the RS, IS, and FS, respectively.



FIG. 3. Action potential properties of the typical RS, IS, and FS neurons in monkey DLPFC. *A–C*: illustration of the shallowest, intermediate and the deepest AHP in RS, IS, and FS, respectively. In addition the RS has afterdepolarization (ADP) and slow components of afterhyperpolarization (AHPs) that are lacking in the IS and FS. *D–F*: action potential as illustrated from threshold (T) is the largest and widest in the RS (*D*) and the smallest and fastest in the FS (*F*). Action potential in the IS displays the properties that are intermediate in values (*E*).

Morphological description of the recorded neurons

A total of 159 neurons were morphologically identified, including 23 pyramidal and 136 nonpyramidal cells. Long duration of recording and of filling with biocytin allowed us to recover a detailed morphology for most of the neurons (Fig. 6). The high quality of the morphological recovery was often evidenced by the fact that individual axon collaterals stopped abruptly inside the section with no gradual reduction of the labeling. Pyramidal cells had clear apical and basal dendrites that were densely covered with spines. Dendrites of interneurons on the other hand almost always lacked spines. For interneurons, we adopted the original classification of interneurons in the monkey DLPFC based on Golgi impregnations (Lund and Lewis 1993). This classification mostly relies on the axonal arborization of these cells because the dendritic morphology is less discriminating across interneurons (Fairen et al. 1984). Because neurogliaform, vertically oriented (correspond to double-bouquet cells) and chandelier cells display distinct morphological features they have been described solely qualitatively.

Neurogliaform interneurons ($n = 14$) had a distinctive dendritic tree (Fig. 7A). Short, multiple dendrites of these cells spread radially from a small, round soma in all directions, making neurogliaform interneurons similar in appearance to astroglial cells. The dendrites often bifurcated proximally and had frequent regular swellings along their radial course. The axonal arbor of neurogliaform interneurons was spherical in shape, two to three times wider than the extent of the dendritic tree, and horizontally reached widths of about $300 \mu\text{m}$. A distinct feature of the axons of neurogliaform cells was their dense plexus of very fine branches, which resembled spider webs.

Vertically oriented cells (also referred to as double-bouquet cells; $n = 35$) had axons with a predominantly vertical extent (Fig. 7B). The axons spanned several layers, often reaching from layer 1 to layers 5–6. The vertical dimension of the axonal arbor considerably exceeded its horizontal extent. The latter was defined by multiple, short, predominantly horizontal, simple processes stemming from several long, vertical, coarse axons. The total width of the arbor usually ranged between 150 and $300 \mu\text{m}$. Cell bodies of vertically oriented interneurons were relatively small, oval in shape, and vertically oriented. Dendrites usually originated from both poles of the soma, either as simple processes or as stems, that branched proximally up to two times before giving off long, simple, terminal branches.

Another large group of cells constituted arbor (basket) cells. A distinct feature of these interneurons was that the horizontal dimension of their axonal arbors was equal to or considerably exceeded the vertical dimension. We followed the previous morphological description (Lund and Lewis 1993) and grouped these cells based on their horizontal axonal spread into local ($n = 24$), medium ($n = 26$), and wide arbor cells ($n = 25$) (Fig. 8). The horizontal extent of axons for local arbor cells was $474 + 77 \mu\text{m}$ ($n = 6$), for medium arbor cells was $662 + 118 \mu\text{m}$ ($n = 6$), and for wide arbor cells was $1038 + 179 \mu\text{m}$ ($n = 4$). In general the axons of arbor cells were confined within the layer containing its soma (layer 2 or 3) and did not spread into layer 1. A single vertical branch of the axon often descended to layer 5. When compared with neurogliaform interneurons, the axonal density of arbor cells was considerably lower and their axons had thicker branches covered with larger boutons. The somata of these cells usually were larger than those of neurogliaform interneurons and vertically oriented interneurons and had an oval or circular shape. Several long dendrites extended from the cell body without a preferred direction, either as simple processes or as stems bifurcating proximally one or two times before conversion to long terminal dendrites.

Chandelier cells ($n = 12$) had a narrow axonal span (about $200\text{-}\mu\text{m}$ horizontal spread) with multiple axonal cartridges arranged in a classical vertical manner known to target the axonal initial segments of pyramidal cells (Fig. 8). Chandelier interneurons had small somata and smooth dendrites. The latter were relatively straight and vertically arranged.

Correspondence of intrinsic membrane properties and morphology

After the morphology of each neuron was identified, we mapped them into the previously obtained dendrogram with the physiological clusters to assess potential structure–functional correlations. Of the 159 morphologically identified neurons, only 111 were included in the dendrogram because the cluster analysis excluded the remaining 48 neurons as a result of at least one missing variable. The distribution of the five major morphological classes of cortical neurons across the three physiologically defined clusters is shown in Fig. 9. Of the pyramidal cells 100% were RS and of the chandelier cells 100% were FS neurons (Fig. 9A). The remaining three morphological groups contained a mix of physiological types. Although the composition of the latter differed substantially across the morphological groups, the majority of arbor cells were FS cells, whereas the majority of vertically oriented cells

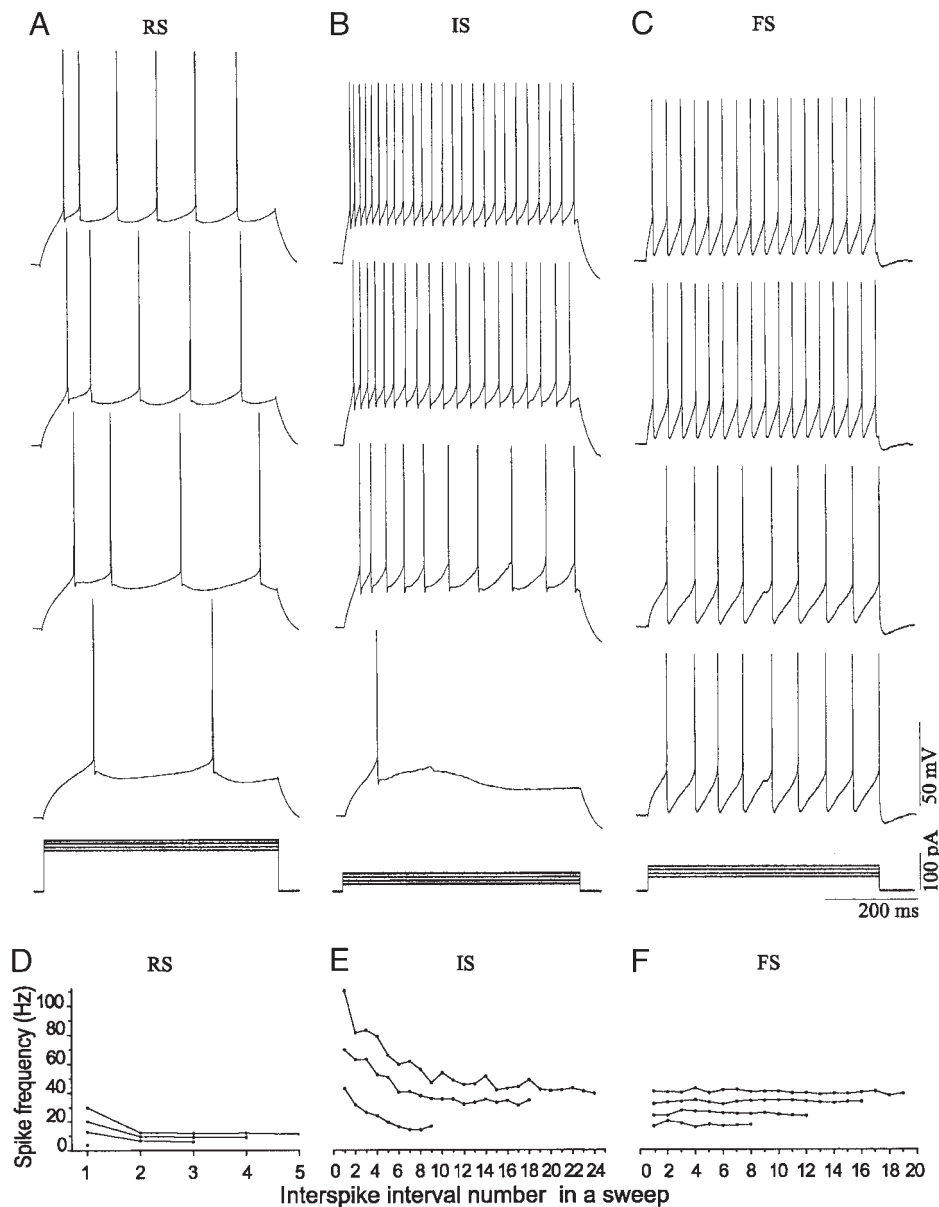


FIG. 4. A–C: subsequent sweeps with spikes beginning with the response to the first supra-threshold current step recorded from the typical RS, IS, and FS neurons in monkey DLPFC. D–F: plots of spike frequencies in the sweeps illustrated in A–C. After the stimulating current reached spike threshold in each of the 3 cells 4 current steps, each of 10 pA were applied. In response to the same intensities of current RS generated the smallest number of spikes at the lowest frequency and with noticeable frequency accommodation. Degree of accommodation moderately increased with increase in current intensity. RS also required the largest current to reach threshold. Of note, 2 different RSs depicted here and in Fig. 2A. FS generated a large number of spikes at high frequencies with no frequency accommodation across the applied current range, requiring less current to reach spike threshold compared with RS. Of note, 2 different FSs are depicted here and in Fig. 2C. IS also generated a large number of spikes at high frequencies, but with prominent frequency accommodation. IS required the smallest current to reach spike threshold.

were IS interneurons. Neurogliaform interneurons consisted of a nearly even mix of RS and IS cells (Fig. 9A). Figure 9B describes the morphological composition of the three physiological classes. It is important to note, however, that this morphological composition is biased by the number of neurons in each morphological group. The cluster of RS cells contained 70% pyramidal, 15% neurogliaform, 9% vertically oriented, and 6% arbor cells. Because the numbers of pyramidal, neu-

rogliaform, vertically oriented, and arbor cells in this study were 23, 14, 35, and 75, respectively, it is expected that the real percentages of pyramidal and neurogliaform cells are higher, whereas the percentages of vertically oriented and, especially, of arbor cells should be lower in the RS cluster. The IS cluster contained no pyramidal cells, 15% neurogliaform, 55% vertically oriented, and 33% arbor cells. Again, it is expected that the percentage of neurogliaform cells is higher, whereas that of arbor cells is lower in this cluster. Finally, the FS cluster, in addition to arbor and chandelier cells, contained 18% of vertically oriented interneurons.

We also looked for potential physiological differences in the individual morphological types of interneurons. In this regard, local, medium, wide arbor, and chandelier cells were very homogeneous even across substantially different morphologies such as wide arbor cells and chandelier interneurons (Table 3). In contrast, there were statistical differences between neurogliaform and vertically oriented cells (Fig. 10). The slope of

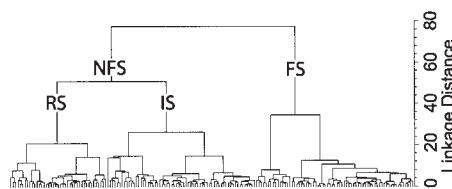


FIG. 5. Cluster analysis of the physiological properties of neurons in monkey DLPFC. Depicted dendrogram clearly segregated RS, IS, and FS clusters as having large linkage distances. NFS (non-FS) cluster was introduced to contrast RS and IS groups with FS cluster.

TABLE 2. *Physiological properties of neuronal clusters*

No.	Variable	RS (n = 41)	IS (n = 63)	FS (n = 67)	F-ratio	Fisher LSD
1	RMP, mV	-73 ± 5	-76 ± 6	-74 ± 5	5.6	(RS = FS) > IS
2	RI, mΩ	263 ± 183	626 ± 312	291 ± 143	46	(RS = FS) < IS
3	TC, ms	17 ± 6.1	17.1 ± 7.7	11.3 ± 5.9	15	(RS = IS) > FS
4	APT, mV	-40 ± 5	-44 ± 8	-43 ± 4	4.8	RS > (IS = FS)
5	APA, mV	78 ± 14.0	66 ± 12.4	54 ± 11.2	46	RS > IS > FS
6	APD, ms	0.73 ± 0.15	0.67 ± 0.15	0.37 ± 0.09	123	RS > IS > FS
7	AHPaf, mV	13.6 ± 4.2	16.2 ± 6.0	21.5 ± 4.9	34	RS < IS < FS
8	AHPAs, mV	1.63 ± 1.71	0.08 ± 0.27	0.25 ± 0.69	31	RS > (IS = FS)
9	ADPA, mV	5.26 ± 3.50	1.17 ± 2.52	1.84 ± 2.24	37	RS > (IS = FS)
10	AR	0.47 ± 0.18	0.59 ± 0.21	0.82 ± 0.21	42	RS < IS < FS
11	Slope × 10 ⁻³	-3.83 ± 2.82	-0.64 ± 2.22	0.46 ± 1.89	47	RS < IS < FS
12	TTP, ms	127 ± 70	70 ± 68	129 ± 147	6.0	(RS = FS) > IS

Statistical significance at $P < 0.05$. Abbreviations are the same as in Table 1.

adaptation ratios across a range of injected currents was severalfold more negative for neurogliaform interneurons than it was for vertically oriented or for arbor and chandelier cells ($P < 0.001$; Figs. 10 and 11). Neurogliaform interneurons also showed prominent AHPs (Figs. 10 and 11A) that neither vertically oriented nor arbor and chandelier cells had ($P < 0.001$). Finally, neurogliaform cells generated a high frequency of initial spikes in the sweeps, which contrasted with consid-

erably lower frequency of the remaining spikes of the sweeps (Fig. 11B).

Unusual firing patterns of interneurons

We encountered several rare firing patterns among the interneurons. Nine interneurons displayed a mixed firing pattern (Fig. 12, A and B). Their first interspike interval was equal to

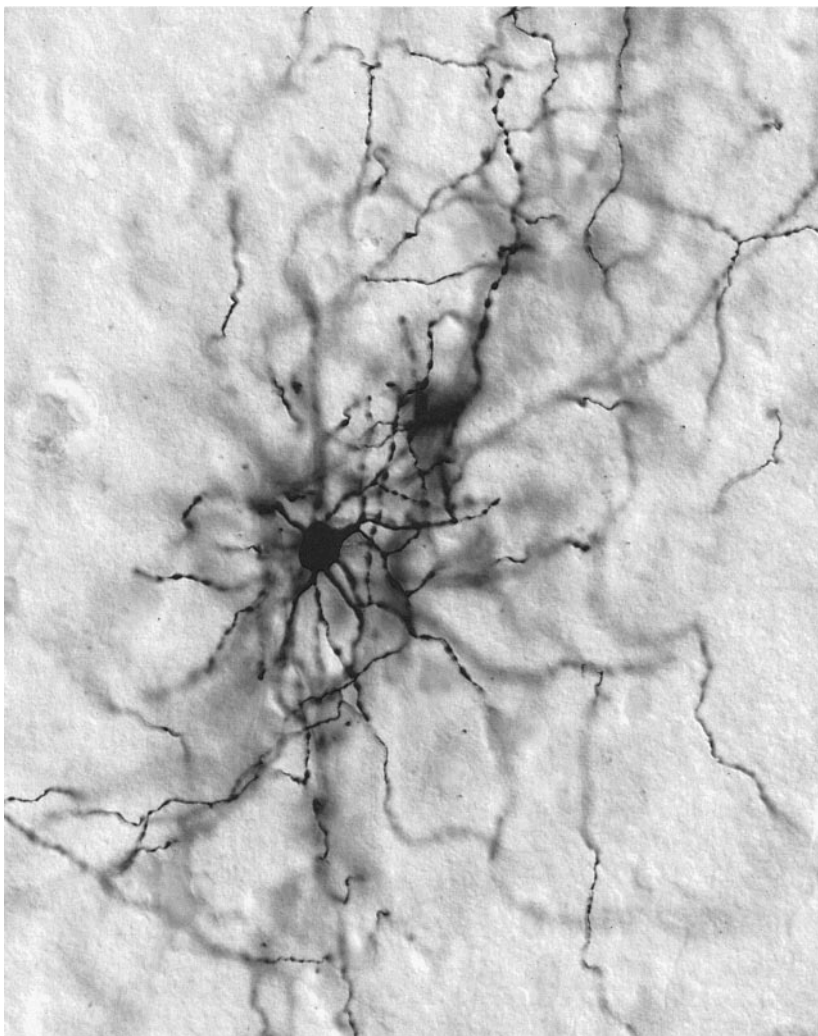


FIG. 6. Brightfield photomicrograph of biocytin-labeled neurogliaform interneuron.

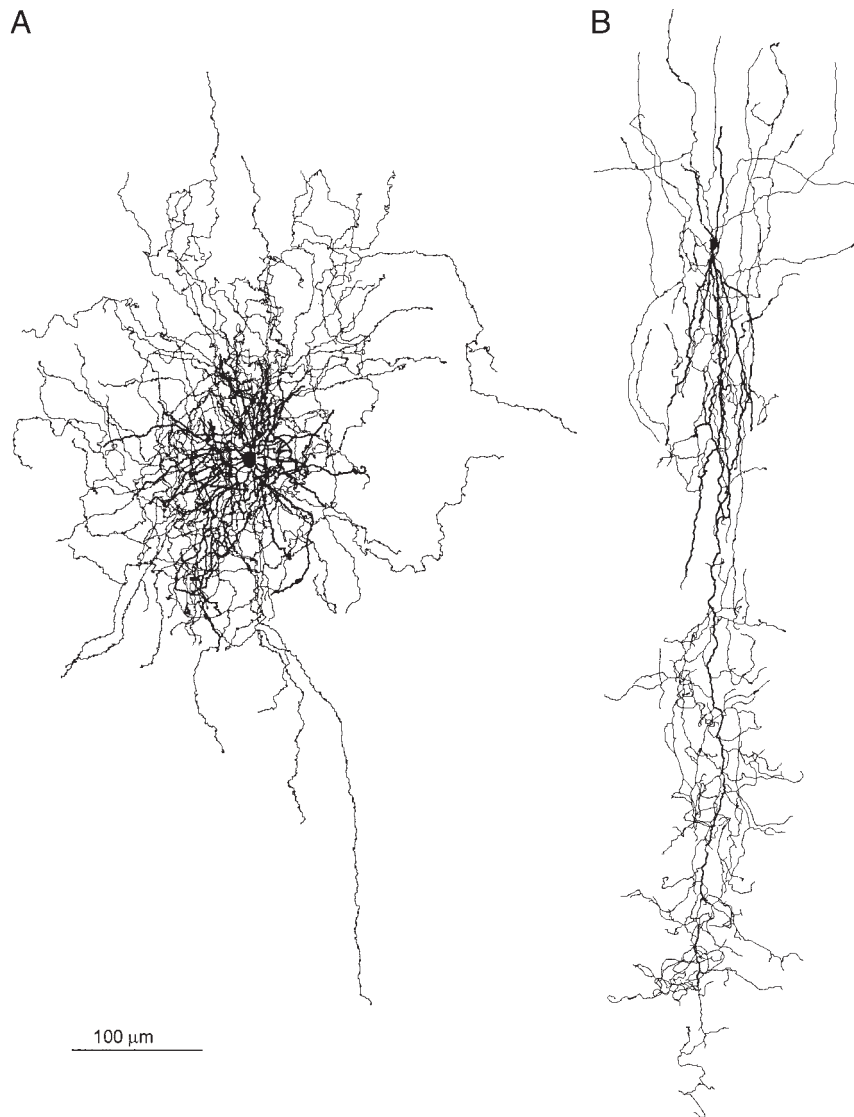


FIG. 7. Morphological varieties of IS cluster. *A*: neurogliaform interneuron (NGF). *B*: vertically oriented interneuron (VO). See RESULTS for the detailed description of the neurons.

the last one, so that the adaptation ratio, if calculated, was close to 1. However, the second interspike interval was considerably narrower than the first one, and there was a noticeable spike adaptation beginning from the second interspike interval. This pattern was consistent across all sweeps evoked by the current steps of subsequently increasing intensity (Fig. 12*B*). Five interneurons with such mixed firing properties were morphologically identified: four as vertically oriented and one as local arbor cells. Both the latter and the other six interneurons with mixed firing pattern still fell in the IS cluster, despite their adaptation ratio characteristic for FS cells. However, one vertically oriented cell and one interneuron with unidentified morphology appeared in the FS cluster.

Interneurons with bursting firing properties were extremely rare in our sample. We encountered only two cells of this type. One of the interneurons produced a burst of spikes on a prominent depolarization ramp (Fig. 12*C*). This cell was mapped into the IS cluster. Morphologically, this neuron had a small, vertically oriented oval soma and bitufted dendrites; the axon was not recovered. The other interneuron also produced a burst of spikes, but on a less prominent ramp of depolarization (Fig. 12*D*). Morphologically, this interneuron had dendrites

moderately covered with spines and multiple axonal branches in layer 1. Although not included in the cluster analysis, this neuron also displayed membrane properties consistent with IS cells. Chandelier interneurons, although all FS, in several instances displayed late spiking features with a prominent depolarization ramp and initial spikes generated at the end of the sweeps evoked with low-stimulation current (Fig. 12, *E* and *F*), whereas at high-stimulus currents these cells fired from the beginning of the sweep without significant spike frequency adaptation. In contrast, neurogliaform interneurons generated their first spikes at the onset of the first suprathreshold sweep. The latter lacked a depolarization ramp.

DISCUSSION

We have successfully applied cluster analysis to segregate RS, IS, and FS groups of neurons in the monkey DLPFC and have provided statistical evidence that the cortical interneurons are not composed of cells with a continuum of physiological properties. The segregation of interneurons based on physiological properties was strongly supported by morphological differences. For example, all of the chandelier cells had FS

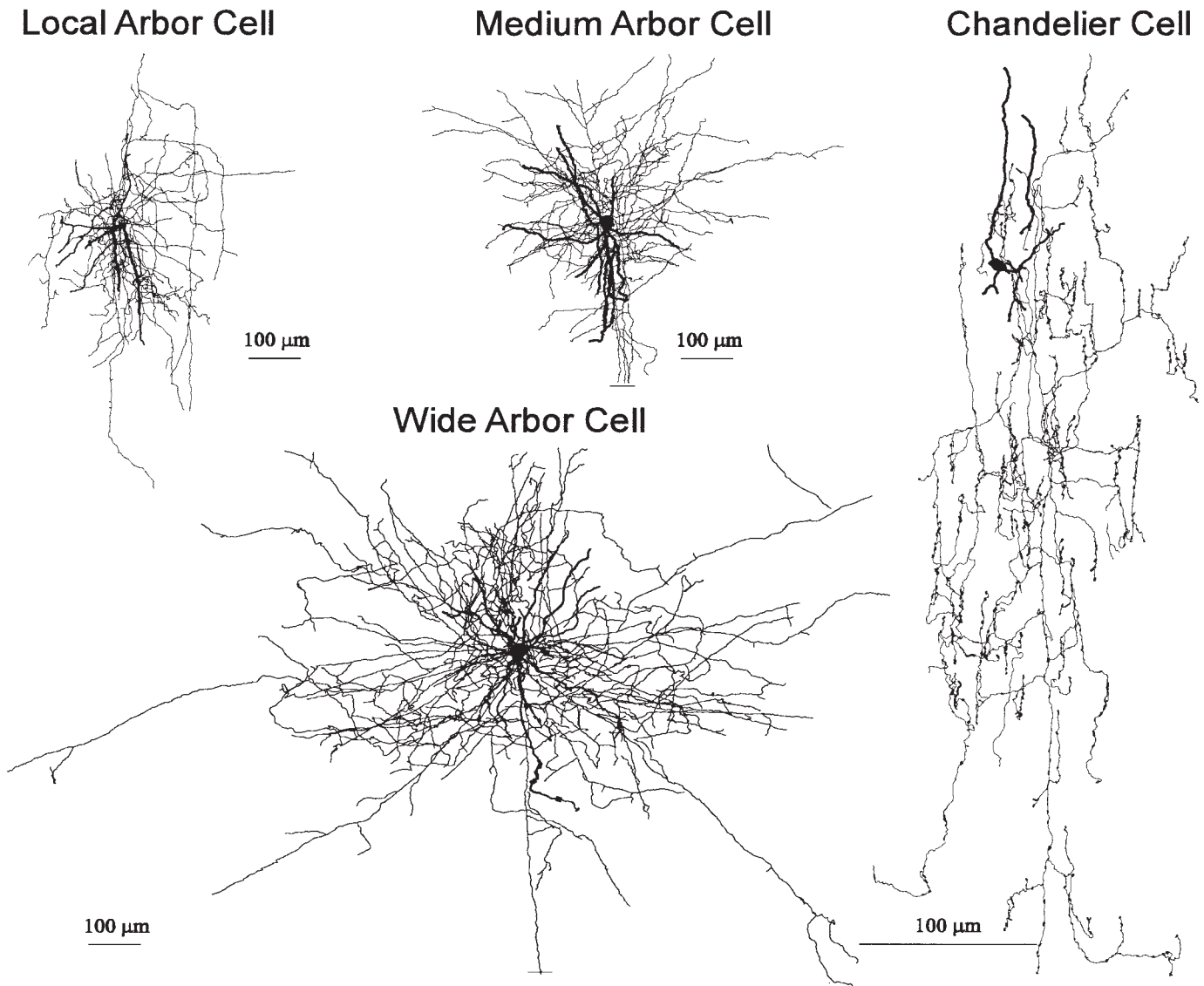


FIG. 8. Morphological varieties of FS cluster. See RESULTS for the detailed description of the neurons.

properties, whereas none of the neurogliaform interneurons did. Finally, the combination of electrophysiological and morphological properties suggests the existence of five major classes of interneurons: RS or IS neurogliaform interneurons, IS vertically oriented cells, FS chandelier, and FS arbor cells.

Physiological classification of interneurons

Extracellular spiking properties are typically the only data that can be obtained by *in vivo* recordings from primate cortex. Thus studying the intrinsic electrophysiological properties of neurons in detail in a cortical slice preparation is essential for interpreting *in vivo* data (González-Burgos et al. 2005). To this end, we showed here that the RS and FS units identified *in vivo* in monkey DLPFC (Constantinidis et al. 2002; Rao et al. 1999) are, indeed, distinct electrophysiological entities. Furthermore, our study demonstrated that although the spike width measure used in the *in vivo* studies appeared to be the best discriminating criterion between groups of neurons, the distribution of spike widths for IS cells considerably overlaps with that of

either RS or FS neurons. Thus additional physiological criteria are needed to accurately segregate these groups. Based on our data (Table 2) cells with spike durations <0.4 ms can be expected to be all FS interneurons. However, our study shows no clear cutoff values of spike width between IS and RS groups. Therefore these groups may be less readily identifiable *in vivo* solely on the basis of spike width.

We have also shown that physiological clusters of neurons in monkey DLPFC to a certain degree predicted their morphologies. For example, FS interneurons were most likely to be arbor or chandelier cells, whereas IS interneurons predominantly had vertically oriented and neurogliaform morphologies. Because arbor and chandelier cells versus vertically oriented and neurogliaform interneurons have been shown to have distinct postsynaptic targets and inhibitory functions in other animal species (Cobb et al. 1995; Larkum et al. 1999; Maccaferri et al. 2000; McBain and Fisahn 2001; Miles et al. 1996; Somogyi et al. 1977, 1981, 1983, 1998; Tamas et al. 1997, 2003), it is possible that the postsynaptic targets and the inhibitory functions of

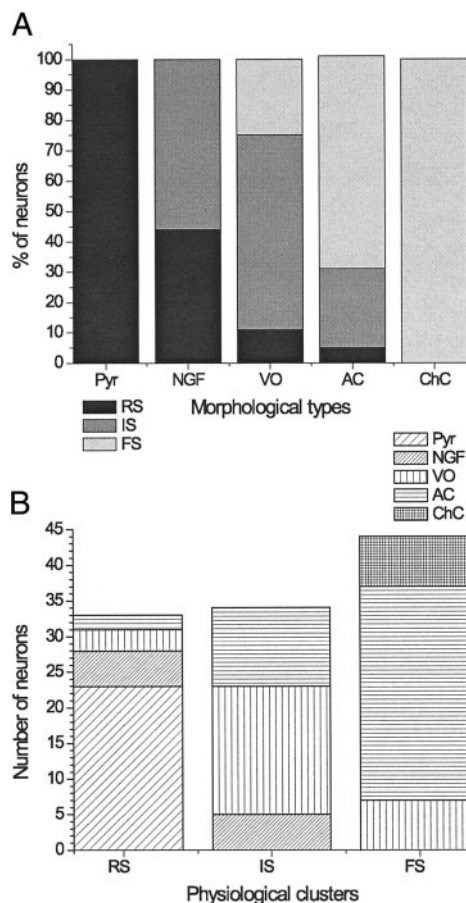


FIG. 9. Morphological representation of the physiological clusters. *A*: percentage of neurons out of total number of the neurons in each morphological type that fell in RS, IS, or FS cluster. *B*: number of neurons of each morphological type in RS, IS, and FS physiological clusters. See RESULTS for more detailed description. Abbreviations: Pyr, pyramidal cells; NGF, neurogliaform interneurons; VO, vertically oriented interneurons; AC, arbor (basket) cells; ChC, chandelier cells.

interneurons in monkey DLPFC might be also inferred from their electrophysiological identification as FS or IS.

Terminology used for the physiological classification of neurons

A classification of cortical neurons as regular- or fast-spiking cells (Mountcastle et al. 1969; Simons 1978), corre-

sponding to pyramidal and nonpyramidal neurons, respectively (McCormick et al. 1985), has been used for decades. In subsequent in vitro studies of the prefrontal cortex, the term “fast-spiking cell” was assigned to only a subpopulation of interneurons with the shortest spikes and nonadapting firing properties (Kawaguchi 1993), whereas the other often encountered a subset of interneurons with wider spikes and adapting firing patterns was designated as regular-spiking nonpyramidal cells (Kawaguchi 1995; Kawaguchi and Kubota 1997). This classification has been widely used (Bacci et al. 2003; Dantzer and Callaway 2000; Gao et al. 2003; Gorelova et al. 2002; Karube et al. 2004; Krimer and Goldman-Rakic 2001; Pawelzik et al. 2002; Porter et al. 2001). The term “regular-spiking nonpyramidal cell” could not be used in our physiological cluster because the latter could include pyramidal cells. Thus we used the term IS because many properties of these neurons had values intermediate between RS and FS cells (Table 2). An alternative terminology based on spike adaptation, rather than on spike width, has been used to designate groups of interneurons as nonadapting or nonaccommodating versus adapting or accommodating types (Chitwood and Jaffe 1998; Gupta et al. 2000; Reyes et al. 1998; Wang et al. 2002). In this study we used the terminology based on spike width because it appeared to be the most discriminating criterion between the clusters, with an F-ratio almost three times larger than for any other physiological variables (Table 2).

Correlation of physiological and morphological properties of interneurons

Our results provide strong evidence that classes of neurons defined by electrophysiological membrane properties correspond with morphological types of neurons. Neurons that had specific and easily recognizable morphological features appeared to have a perfect match with the corresponding physiological clusters. For example, 100% of pyramidal cells fell in RS cluster, 100% of chandelier cells were in FS cluster, and 100% of neurogliaform cells were included in the more general non-FS cluster, indicating that none of the neurogliaform interneurons displayed FS physiological properties. Arbor and vertically oriented cells demonstrated more diverse structure–functional correspondence, perhaps as a result of significant molecular diversity among the interneurons of similar morphological types (Cauli et al. 1997; Markram et al. 2004; Pawelzik et al.

TABLE 3. *Physiological properties of morphologically identified FS*

No.	Variable	L (n = 24)	M (n = 26)	W (n = 25)	C (n = 12)	Fisher Post hoc
1	RMP, mV‡	-72 ± 7	-75 ± 6	-72 ± 5	-70 ± 6	L = M = W = C
2	RI, mΩ‡	392 ± 293	405 ± 256	297 ± 146	379 ± 172	L = M = W = C
3	TC, ms‡	13.8 ± 6.1	12 ± 4.8	8.4 ± 2.2	9.4 ± 2.2	L = M; M = C; W = C
4	APT, mV	-44 ± 7	-42 ± 6	-43 ± 4	-45 ± 3	L = M = W = C
5	APA, mV	54 ± 17.8	53 ± 13.8	53 ± 13.2	55 ± 9.6	L = M = W = C
6	APD, ms	0.43 ± 0.12	0.46 ± 0.16	0.44 ± 0.19	0.34 ± 0.10	L = (M > C) = W
7	AHPAf, mV‡	21.1 ± 5.7	20.8 ± 5.6	21.9 ± 5.6	18.4 ± 3.7	L = M = W = C
8	AHPAs, mV‡	1.45 ± 2.05	1.61 ± 2.63	1.90 ± 2.21	1.57 ± 1.96	L = M = W = C
9	ADPAf, mV‡	0.84 ± 2.29	0.45 ± 0.79	0.48 ± 0.84	0.17 ± 0.45	L = M = W = C
10	AR	0.88 ± 0.22	0.76 ± 0.20	0.84 ± 0.15	0.93 ± 0.16	[(L = C) < M] = W
11	Slope × 10 ⁻³	-0.27 ± 2.02	0.44 ± 2.11	0.01 ± 1.63	-0.80 ± 1.83	L = M = W = C
12	TTP, ms	159 ± 156	65 ± 60	60 ± 59	207 ± 212	(L = C) > (M = W)

Statistical significance at *P* < 0.05. L, M, W, and C, local, medium, wide arbor, and chandelier cells, respectively. ‡n = 14, 14, 15, and 7 for L, M, W, and C, respectively. Abbreviations are the same as in Table 1.

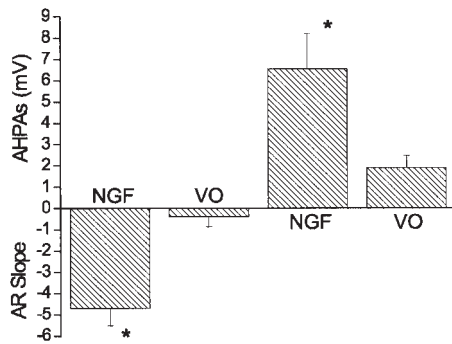


FIG. 10. Differences in the physiological membrane properties between NGF and VO cells. Statistically significant differences ($P < 0.0001$) were in the slope of adaptation ratio (AR Slope) and in amplitude of the AHPs.

2002). Our cluster analysis has suggested that there might be additional subgroups among the FS and IS clusters, which could correspond to specific molecular markers of the interneurons, distinct postsynaptic receptors, or other factors. Without this information, however, further subdivision of the subclusters in our study could not be meaningfully supported. Indeed, it is intriguing to note that local, medium, and wide arbor cells not only represent the majority of the cells in the FS cluster, but also displayed almost identical intrinsic membrane properties, including those related to the temporal properties of the action potentials. These morphological types of interneurons correspond to basket cells, which constitute a substantial number of inhibitory synapses on soma and proximal dendrites of pyramidal cells (Somogyi et al. 1983; Tamas et al. 2003).

Perisomatic inhibition provided by basket cells evokes considerably stronger inhibitory currents than does dendritic inhibition measured at the soma (Maccaferri et al. 2000). Perisomatic inhibition is thought to regulate synchronous and oscillatory activity of large populations of pyramidal cells (McBain and Fishan 2001; Somogyi and Klausberger 2005). Using this mechanism, local, medium, and wide arbor cells might be involved in a horizontal integration of pyramidal cells' activity in progressively wider cortical territories of the same layer (Krimer and Goldman-Rakic 2001). The fastest action potentials in FS interneurons along with their other properties (i.e., fast presynaptic excitatory postsynaptic potentials [EPSPs] and postsynaptic inhibitory postsynaptic potentials [IPSPs]) may well serve the purpose of quick delivery of the perisomatic inhibitory effects on the excitatory responses in the postsynaptic pyramidal cells. On the other hand, vertically oriented interneurons might be involved in a vertical integration of pyramidal cells' activity as they span over several cortical layers. Double-bouquet cells, however, target distal dendritic shafts and spines of principal cells (Somogyi and Klausberger 2005; Tamas et al. 2003) and thus may use inhibitory mechanisms different from those of basket cells. For example, recent data from the hippocampus suggest that interneurons targeting distal dendrites are recruited by sustained activity (late persistent interneurons) and may have a modulatory role on the firing rate of pyramidal cells as opposed to a role in controlling the spike timing of pyramidal cells, which is provided by FS cells (Mittmann et al. 2004; Pouille and Scanziani 2004).

Although both vertically oriented and neurogliaform interneurons target distal dendrites of pyramidal cells (Tamas et al.

2003), they appeared to provide different types of inhibition. Inhibitory postsynaptic responses evoked in pyramidal cells by neurogliaform interneurons display a slow, γ -aminobutyric acid-B ($GABA_B$)–mediated component lacking in the responses evoked by bitufted interneurons (Tamas et al. 2003). We have demonstrated that vertically oriented and neurogliaform interneurons also differ in several intrinsic physiological properties. The slope of the adaptation ratio for neurogliaform cells was several times more negative than this measurement in vertically oriented interneurons. This implies that the frequency of the initial spike intervals steeply increased relative to the frequency of the remaining spikes with an increase in

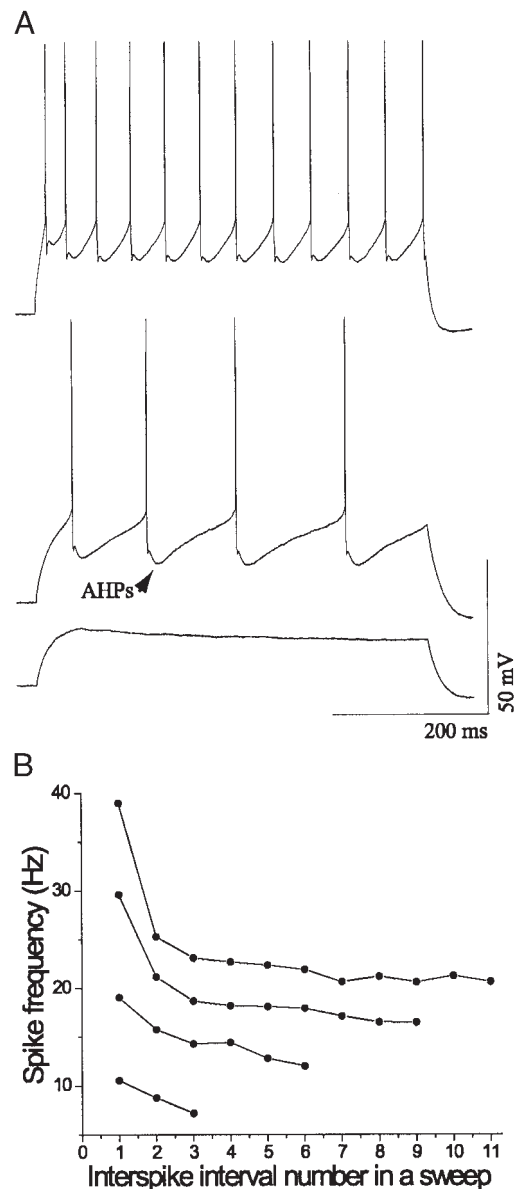


FIG. 11. Physiological properties of neurogliaform interneurons. *A*: subthreshold, 1st, and 4th suprathreshold sweeps evoked by subsequent 10-pA current steps; 2nd and 3rd sweeps are not shown. AHP has a prominent slow component (AHPs). No features of late-spiking cells seem to be present. *B*: spike frequencies are plotted for the 4 suprathreshold cells, including the 2 skipped in *A*. Evoked spike frequencies are relatively low and display prominent adaptation, which increases considerably with increasing stimulating current intensity.

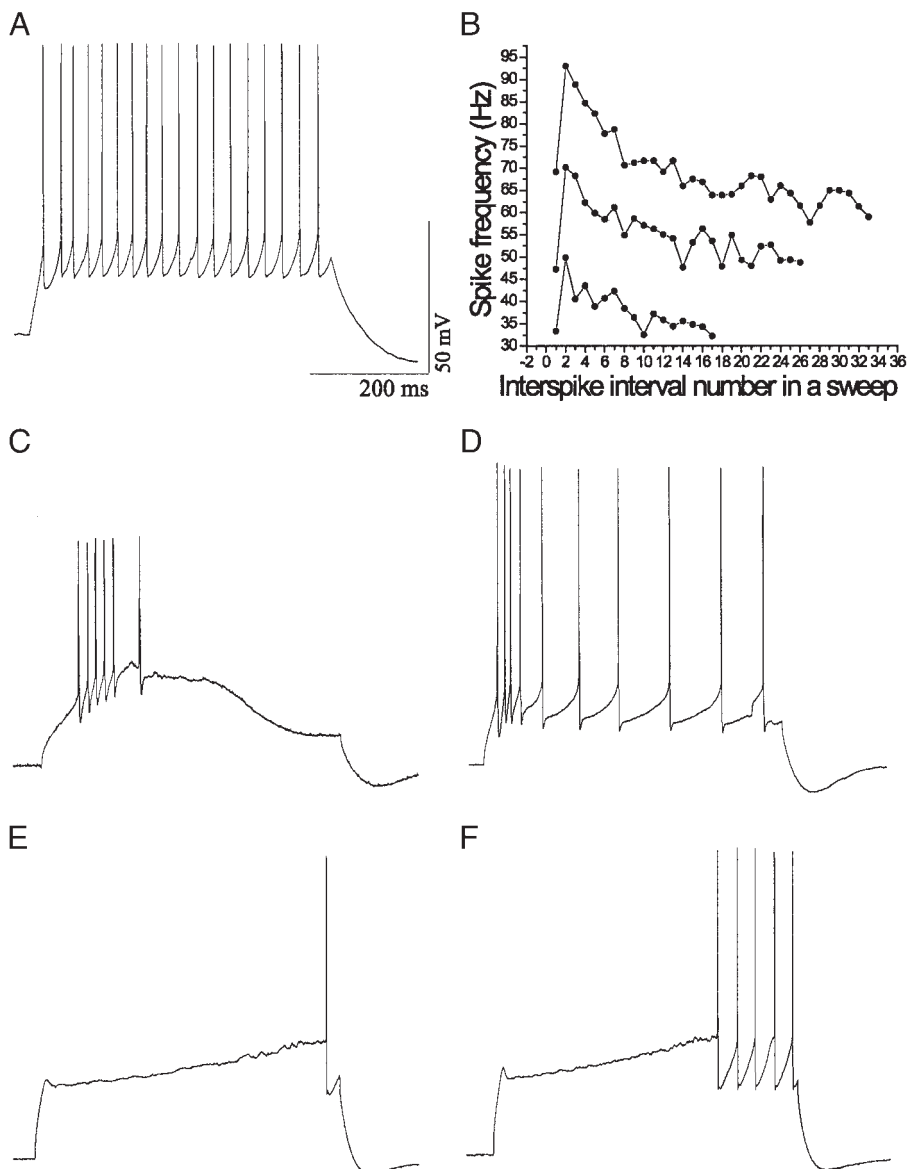


FIG. 12. Examples of unusual firing patterns of interneurons in monkey DLPFC. *A*: this neuron has 1st interspike interval that is similar to the last one; the 2nd interspike interval, however, is considerably shorter and there is a strong frequency adaptation beginning the 2nd interspike interval. *B*: frequency plot of 3 sweeps evoked by the current steps of subsequently increasing intensity from the same neuron. *C* and *D*: only 2 examples of bursting interneurons observed in layers 2–3 from monkey DLPFC. *E* and *F*: example of chandelier cell that generated late spikes on a depolarization ramp. See RESULTS for a more detailed description.

intensity of the stimulating current. Also, the amplitude of AHPs was severalfold larger in neurogliaform than in vertically oriented cells. These distinct features of neurogliaform interneurons made their intrinsic electrophysiological properties the closest to pyramidal cells, so that almost half of neurogliaform and pyramidal cells were grouped together in the RS cluster.

Differences in physiological properties of morphologically identified interneurons between monkey and other species

The physiological properties of neurogliaform interneurons in adult monkey appeared to have an important difference compared with immature (Chu et al. 2003; Kawaguchi 1995; Tamas et al. 2003) and, perhaps, adult rats (Zhu and Zhu 2004). None of our 14 neurogliaform cells displayed late spiking properties described in these studies in rodents (LS cells). Surprisingly, several chandelier cells displayed some features reminiscent of LS cells (Fig. 12, *E* and *F*), although all chandelier interneurons still matched with FS cluster.

In monkey DLPFC, we have not been able to identify a group of low-threshold (LTS) or burst-spiking interneurons typically seen in rat frontal cortex (Kawaguchi 1995; Kawaguchi and Kubota 1997). Only a few cells were found to display these features (Fig. 12, *C* and *D*). We also have described a subgroup of interneurons with an unusual combination of nonadapting and adapting firing patterns, which has not been described in rat PFC. The physiological significance of vertically oriented cells with this firing pattern remains to be investigated. Thus although major similarities in electrophysiological membrane properties of interneurons were found between monkey and rat PFC, there were also important differences.

ACKNOWLEDGMENTS

We thank O. A. Krimer for excellent technical support. Present addresses: G. Czanner, Department of Anesthesia and Critical Care, Massachusetts General Hospital, Boston, MA 02114; S. Kröner, Department of Physiology and Neuroscience, Medical University of South Carolina, Charleston, SC 29425.

GRANTS

This work was supported by National Institute of Mental Health Grants MH-067963, MH-63561, and MH-51234, and National Alliance for Research on Schizophrenia to G. González-Burgos.

REFERENCES

- Bacci A, Huguenard JR, and Prince DA.** Functional autaptic neurotransmission in fast-spiking interneurons: a novel form of feedback inhibition in the neocortex. *J Neurosci* 23: 859–866, 2003.
- Blatow M, Caputi A, Burnashev N, Monyer H, and Rozov A.** Ca²⁺ buffer saturation underlies paired pulse facilitation in calbindin-D28k-containing terminals. *Neuron* 38: 79–88, 2003.
- Cauli B, Audinat E, Lambollez B, Angulo MC, Ropert N, Tsuzuki K, Hestrin S, and Rossier J.** Molecular and physiological diversity of cortical nonpyramidal cells. *J Neurosci* 17: 3894–3906, 1997.
- Cauli B, Porter JT, Tsuzuki K, Lambollez B, Rossier J, Quenet B, and Audinat E.** Classification of fusiform neocortical interneurons based on unsupervised clustering. *Proc Natl Acad Sci USA* 97: 6144–6149, 2000.
- Chitwood RA and Jaffe DB.** Calcium-dependent spike-frequency accommodation in hippocampal CA3 nonpyramidal neurons. *J Neurophysiol* 80: 983–988, 1998.
- Chu Z, Galarreta M, and Hestrin S.** Synaptic interactions of late-spiking neocortical neurons in layer 1. *J Neurosci* 23: 96–102, 2003.
- Cobb SR, Buhl EH, Halasy K, Paulsen O, and Somogyi P.** Synchronization of neuronal activity in hippocampus by individual GABAergic interneurons. *Nature* 378: 75–78, 1995.
- Conde F, Lund JS, Jacobowitz DM, Baimbridge KG, and Lewis DA.** Local circuit neurons immunoreactive for calretinin, calbindin D-28K or parvalbumin in monkey prefrontal cortex—distribution and morphology. *J Comp Neurol* 341: 95–116, 1994.
- Connors BW and Gutnick MJ.** Intrinsic firing patterns of diverse neocortical neurons. *Trends Neurosci* 13: 99–104, 1990.
- Constantinidis C, Williams GV, and Goldman-Rakic PS.** A role for inhibition in shaping the temporal flow of information in prefrontal cortex. *Nat Neurosci* 5: 175–180, 2002.
- Dantzker JL and Callaway EM.** Laminar sources of synaptic input to cortical inhibitory interneurons and pyramidal neurons. *Nat Neurosci* 3: 701–707, 2000.
- Fairen A, DeFelipe J, and Regidor J.** Nonpyramidal neurons. General account. In: *Cerebral Cortex*, edited by Peters A and Jones EG. New York: Plenum Press, 1984.
- Funahashi S, Bruce CJ, and Goldman-Rakic PS.** Mnemonic coding of visual space in the monkey's dorsolateral prefrontal cortex. *J Neurophysiol* 61: 331–349, 1989.
- Fuster JM.** The prefrontal cortex—an update: time is of the essence. *Neuron* 30: 319–333, 2001.
- Gabbott PLA and Bacon SJ.** Local circuit neurons in the medial prefrontal cortex (areas 24a,b,c, 25 and 32) in the monkey. 2. Quantitative areal and laminar distributions. *J Comp Neurol* 364: 609–636, 1996.
- Gabbott PLA, Dickie BGM, Vaid RR, Headlam AJN, and Bacon SJ.** Local-circuit neurones in the medial prefrontal cortex (areas 25, 32, and 24b) in the rat: morphology and quantitative distribution. *J Comp Neurol* 377: 465–499, 1997.
- Gao WJ, Wang Y, and Goldman-Rakic PS.** Dopamine modulation of perisomatic and peridendritic inhibition in prefrontal cortex. *J Neurosci* 23: 1622–1630, 2003.
- Gibson JR, Beierlein M, and Connors BW.** Two networks of electrically coupled inhibitory neurons in neocortex. *Nature* 402: 75–79, 1999.
- Goldman-Rakic PS.** Cellular basis of working memory. *Neuron* 14: 477–485, 1995.
- Gonzalez-Burgos G, Barrionuevo G, and Lewis DA.** Horizontal synaptic connections in monkey prefrontal cortex: an in vitro electrophysiological study. *Cereb Cortex* 10: 82–92, 2000.
- Gonzalez-Burgos G, Krimer LS, Povysheva NV, Barrionuevo G, and Lewis DA.** Functional properties of fast spiking interneurons and their synaptic connections with pyramidal cells in primate dorsolateral prefrontal cortex. *J Neurophysiol* 93: 942–953, 2005.
- Gonzalez-Burgos G, Krimer LS, Urban NN, Barrionuevo G, and Lewis DA.** Synaptic efficacy during repetitive activation of excitatory inputs in primate dorsolateral prefrontal cortex. *Cereb Cortex* 14: 530–542, 2004.
- Gorelova N, Seamans JK, and Yang CR.** Mechanisms of dopamine activation of fast-spiking interneurons that exert inhibition in rat prefrontal cortex. *J Neurophysiol* 88: 3150–3166, 2002.
- Gupta A, Wang Y, and Markram H.** Organizing principles for a diversity of GABAergic interneurons and synapses in the neocortex. *Science* 287: 273–278, 2000.
- Hand DJ.** *Discrimination and Classification*. Chippingham, UK: Wiley, 1981.
- Henze DA, Gonzalez-Burgos GR, Urban NN, Lewis DA, and Barrionuevo G.** Dopamine increases excitability of pyramidal neurons in primate prefrontal cortex. *J Neurophysiol* 84: 2799–2809, 2000.
- Johnson RA and Wichern DW.** *Applied Multivariate Statistical Analysis*. Upper Saddle River, NJ: Prentice Hall, 1998.
- Karube F, Kubota Y, and Kawaguchi Y.** Axon branching and synaptic bouton phenotypes in GABAergic nonpyramidal cell subtypes. *J Neurosci* 24: 2853–2865, 2004.
- Kawaguchi Y.** Groupings of nonpyramidal and pyramidal cells with specific physiological and morphological characteristics in rat frontal cortex. *J Neurophysiol* 69: 416–431, 1993.
- Kawaguchi Y.** Physiological subgroups of nonpyramidal cells with specific morphological characteristics in layer II/III of rat frontal cortex. *J Neurosci* 15: 2638–2655, 1995.
- Kawaguchi Y and Kubota Y.** GABAergic cell subtypes and their synaptic connections in rat frontal cortex. *Cereb Cortex* 7: 476–486, 1997.
- Krimer LS and Goldman-Rakic PS.** Prefrontal microcircuits: membrane properties and excitatory input of local, medium, and wide arbor interneurons. *J Neurosci* 21: 3788–3796, 2001.
- Larkum ME, Zhu JJ, and Sakmann B.** A new cellular mechanism for coupling inputs arriving at different cortical layers. *Nature* 398: 338–341, 1999.
- Letinic K, Zoncu R, and Rakic P.** Origin of GABAergic neurons in the human neocortex. *Nature* 417: 645–649, 2002.
- Lund JS and Lewis DA.** Local circuit neurons of developing and mature macaque prefrontal cortex: Golgi and immunocytochemical characteristics. *J Comp Neurol* 328: 282–312, 1993.
- Maccaferri G, Roberts JD, Szucs P, Cottingham CA, and Somogyi P.** Cell surface domain specific postsynaptic currents evoked by identified GABAergic neurones in rat hippocampus in vitro. *J Physiol* 524: 91–116, 2000.
- Magee JC.** A prominent role for intrinsic neuronal properties in temporal coding. *Trends Neurosci* 26: 14–16, 2003.
- Markram H, Toledo-Rodriguez M, Wang Y, Gupta A, Silberberg G, and Wu CZ.** Interneurons of the neocortical inhibitory system. *Nat Rev Neurosci* 5: 793–807, 2004.
- McBain CJ and Fisahn A.** Interneurons unbound. *Nat Rev Neurosci* 2: 11–23, 2001.
- McCormick DA, Connors BW, Lighthall JW, and Prince DA.** Comparative electrophysiology of pyramidal and sparsely spiny stellate neurons of the neocortex. *J Neurophysiol* 54: 782–806, 1985.
- Miles R, Toth K, Gulyas AI, Hajos N, and Freund TF.** Differences between somatic and dendritic inhibition in the hippocampus. *Neuron* 16: 815–823, 1996.
- Miller EK.** The prefrontal cortex and cognitive control. *Nat Rev Neurosci* 1: 59–65, 2000.
- Mittmann W, Chadderton P, and Hausser M.** Neuronal microcircuits: frequency-dependent flow of inhibition. *Curr Biol* 14: R837–R839, 2004.
- Mountcastle VB, Talbot WH, Sakata H, and Hyvarinen J.** Cortical neuronal mechanisms in flutter-vibration studied in unanesthetized monkeys. Neuronal periodicity and frequency discrimination. *J Neurophysiol* 32: 452–484, 1969.
- Nowak LG, Azouz R, Sanchez-Vives MV, Gray CM, and McCormick DA.** Electrophysiological classes of cat primary visual cortical neurons in vivo as revealed by quantitative analyses. *J Neurophysiol* 89: 1541–1566, 2003.
- Parra P, Gulyas AI, and Miles R.** How many subtypes of inhibitory cells in the hippocampus? *Neuron* 20: 983–993, 1998.
- Pawelzik H, Hughes DI, and Thomson AM.** Physiological and morphological diversity of immunocytochemically defined parvalbumin- and cholecystokinin-positive interneurons in CA1 of the adult rat hippocampus. *J Comp Neurol* 443: 346–367, 2002.
- Porter JT, Johnson CK, and Agmon A.** Diverse types of interneurons generate thalamus-evoked feedforward inhibition in the mouse barrel cortex. *J Neurosci* 21: 2699–2710, 2001.
- Pouille F and Scanziani M.** Routing of spike series by dynamic circuits in the hippocampus. *Nature* 429: 717–723, 2004.
- Povysheva NV, Gonzalez-Burgos G, Zaitsev AV, Kroner S, Barrionuevo G, Lewis DA, and Krimer LS.** Properties of excitatory synaptic responses in fast-spiking interneurons and pyramidal cells from monkey and rat prefrontal cortex. *Cereb Cortex* In press.

- Rao SG, Williams GV, and Goldman-Rakic PS.** Isodirectional tuning of adjacent interneurons and pyramidal cells during working memory: evidence for microcolumnar organization in PFC. *J Neurophysiol* 81: 1903–1916, 1999.
- Reyes A, Lujan R, Rozov A, Burnashev N, Somogyi P, and Sakmann B.** Target-cell-specific facilitation and depression in neocortical circuits. *Nat Neurosci* 1: 279–285, 1998.
- Rozov A, Jerecic J, Sakmann B, and Burnashev N.** AMPA receptor channels with long-lasting desensitization in bipolar interneurons contribute to synaptic depression in a novel feedback circuit in layer 2/3 of rat neocortex. *J Neurosci* 21: 8062–8071, 2001.
- Simons DJ.** Response properties of vibrissa units in rat SI somatosensory neocortex. *J Neurophysiol* 41: 798–820, 1978.
- Somogyi P.** A specific “axo-axonal” interneuron in the visual cortex of the rat. *Brain Res* 136: 345–350, 1977.
- Somogyi P and Cowey A.** Combined Golgi and electron microscopic study on the synapses formed by double bouquet cells in the visual cortex of the cat and monkey. *J Comp Neurol* 195: 547–566, 1981.
- Somogyi P, Kisvarday ZF, Martin KA, and Whitteridge D.** Synaptic connections of morphologically identified and physiologically characterized large basket cells in the striate cortex of cat. *Neuroscience* 10: 261–294, 1983.
- Somogyi P and Klausberger T.** Defined types of cortical interneurone structure space and spike timing in the hippocampus. *J Physiol* 562: 9–26, 2005.
- Somogyi P, Tamas G, Lujan R, and Buhl EH.** Salient features of synaptic organisation in the cerebral cortex. *Brain Res Brain Res Rev* 26: 113–135, 1998.
- Stuart GJ, Dodt HU, and Sakmann B.** Patch-clamp recordings from the soma and dendrites of neurons in brain slices using infrared video microscopy. *Pfluegers Arch* 423: 511–518, 1993.
- Tamas G, Buhl EH, and Somogyi P.** Fast IPSPs elicited via multiple synaptic release sites by different types of GABAergic neurone in the cat visual cortex. *J Physiol* 500:715–738, 1997.
- Tamas G, Lorincz A, Simon A, and Szabadics J.** Identified sources and targets of slow inhibition in the neocortex. *Science* 299: 1902–1905, 2003.
- Wang Y, Gupta A, Toledo-Rodriguez M, Wu CZ, and Markram H.** Anatomical, physiological, molecular and circuit properties of nest basket cells in the developing somatosensory cortex. *Cereb Cortex* 12: 395–410, 2002.
- Xu Q, Cobos I, De la Cruz E, Rubenstein JL, and Anderson SA.** Origins of cortical interneuron subtypes. *J Neurosci* 24: 2612–2622, 2004.
- Zaitsev AV, Gonzalez-Burgos G, Povysheva NV, Kroner S, Lewis DA, and Krimer LS.** Localization of calcium-binding proteins in physiologically and morphologically characterized interneurons of monkey dorsolateral prefrontal cortex. *Cereb Cortex* 15: 1178–1186, 2005.
- Zhu Y and Zhu JJ.** Rapid arrival and integration of ascending sensory information in layer 1 nonpyramidal neurons and tuft dendrites of layer 5 pyramidal neurons of the neocortex. *J Neurosci* 24: 1272–1279, 2004.